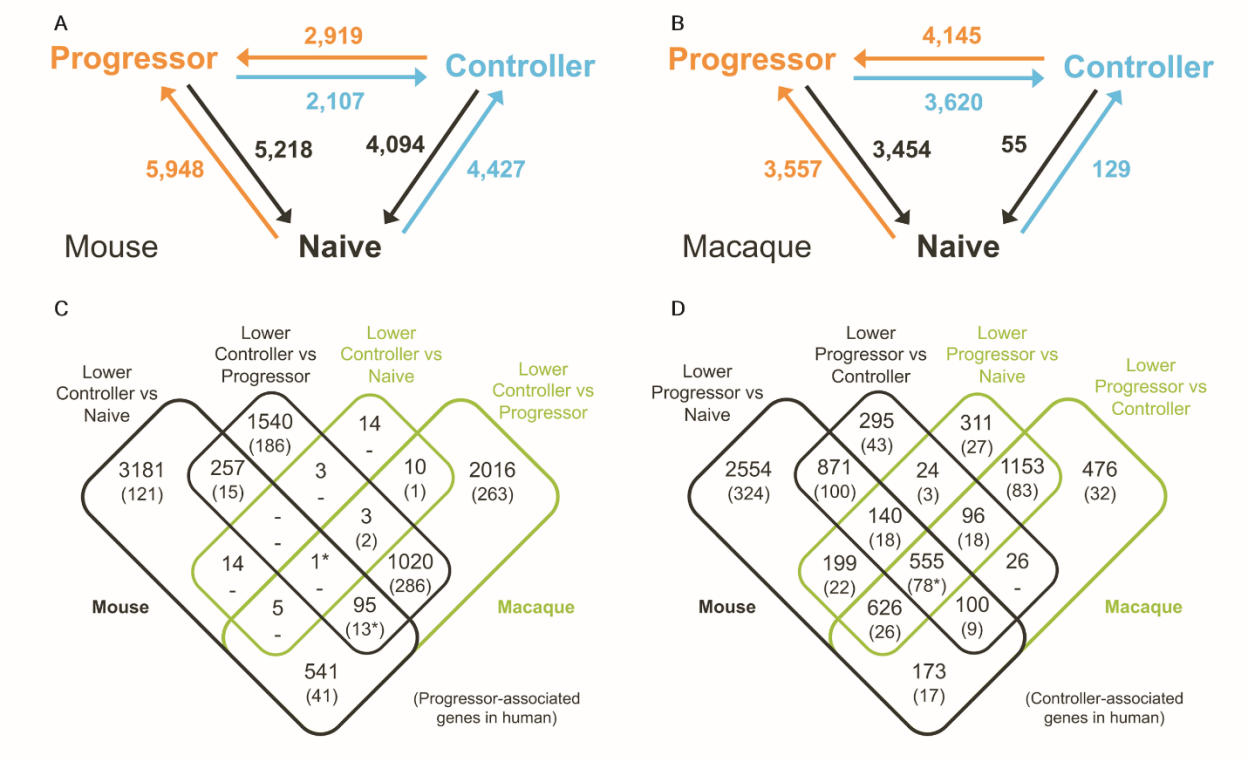

Fig.S1. **Differential gene expression (DESeq2) across species.** Pairwise counts of significantly differentially expressed genes between each sample group are shown for (**A**) mouse and (**B**) macaque. The counts of overlapping differentially expressed genes between mouse genes, macaque genes and human genes (*7*) are shown for all comparisons involving controller and progressor sample sets: (**C**) Genes lower in controller compared to both naïve and progressor samples; (**D**) Genes lower in progressor compared to both naïve and controller samples.*Gene sets visualized in Fig.3.

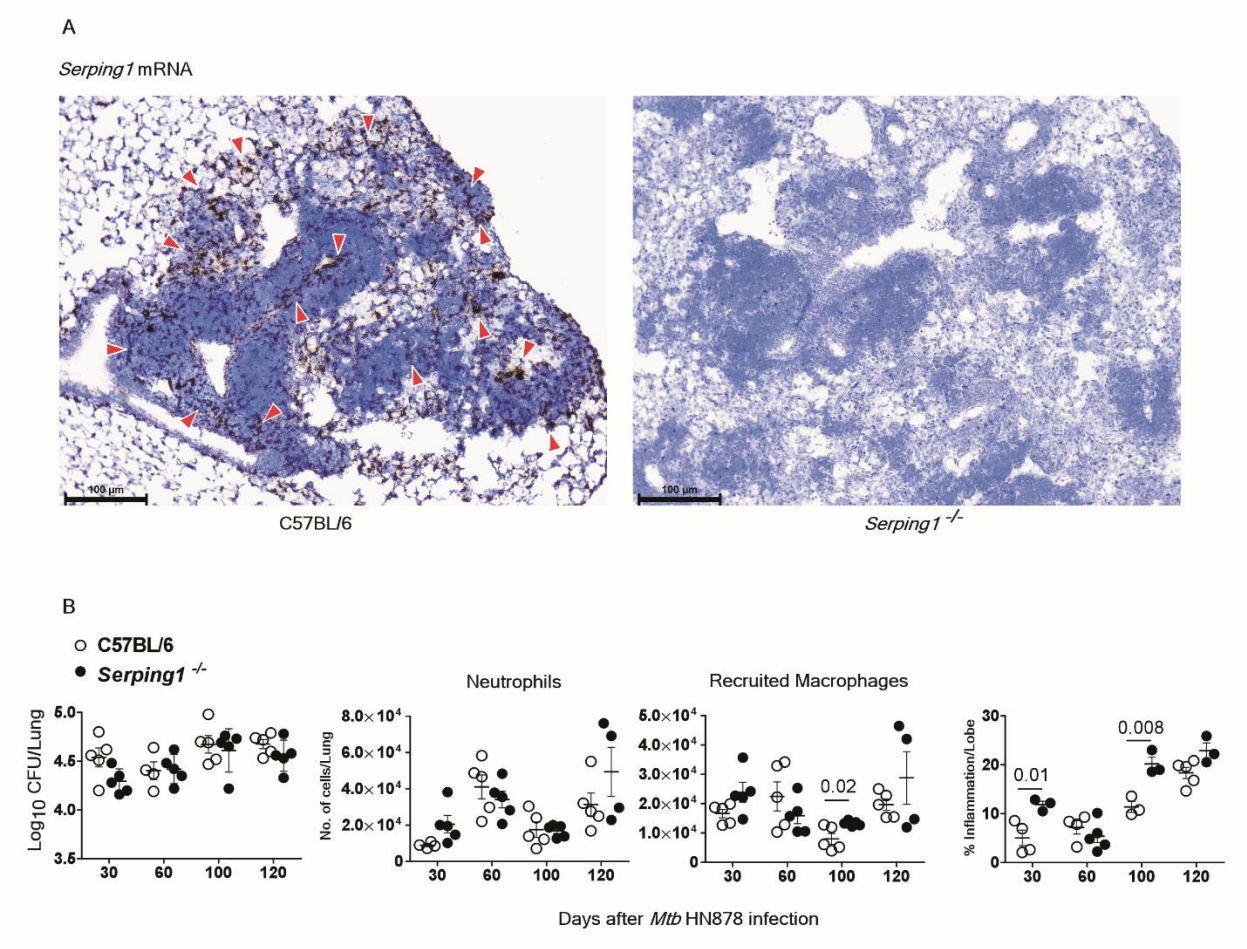

Fig. S2. *Serping1* regulates inflammation but not *Mtb* control in mice. C57BL/6 or *Serping1*$^{-/-}$ mice were challenged with *Mtb* HN878 (100 CFU) by aerosol route and (**A**) *Serping1* mRNA localization was determined within FFPE lung sections using RNAScope. Arrows point to *Serping1* mRNA localization (brown). (**B**) Lungs were harvested to assess bacterial burden or inflammatory cell infiltration by flow cytometry or histologically by H&E staining. The data points represent the means (±SEM) of one out of two separate experiments. *P*-values was determined by unpaired two-tailed Student's t-test between control and gene deficient mice, at different time points.

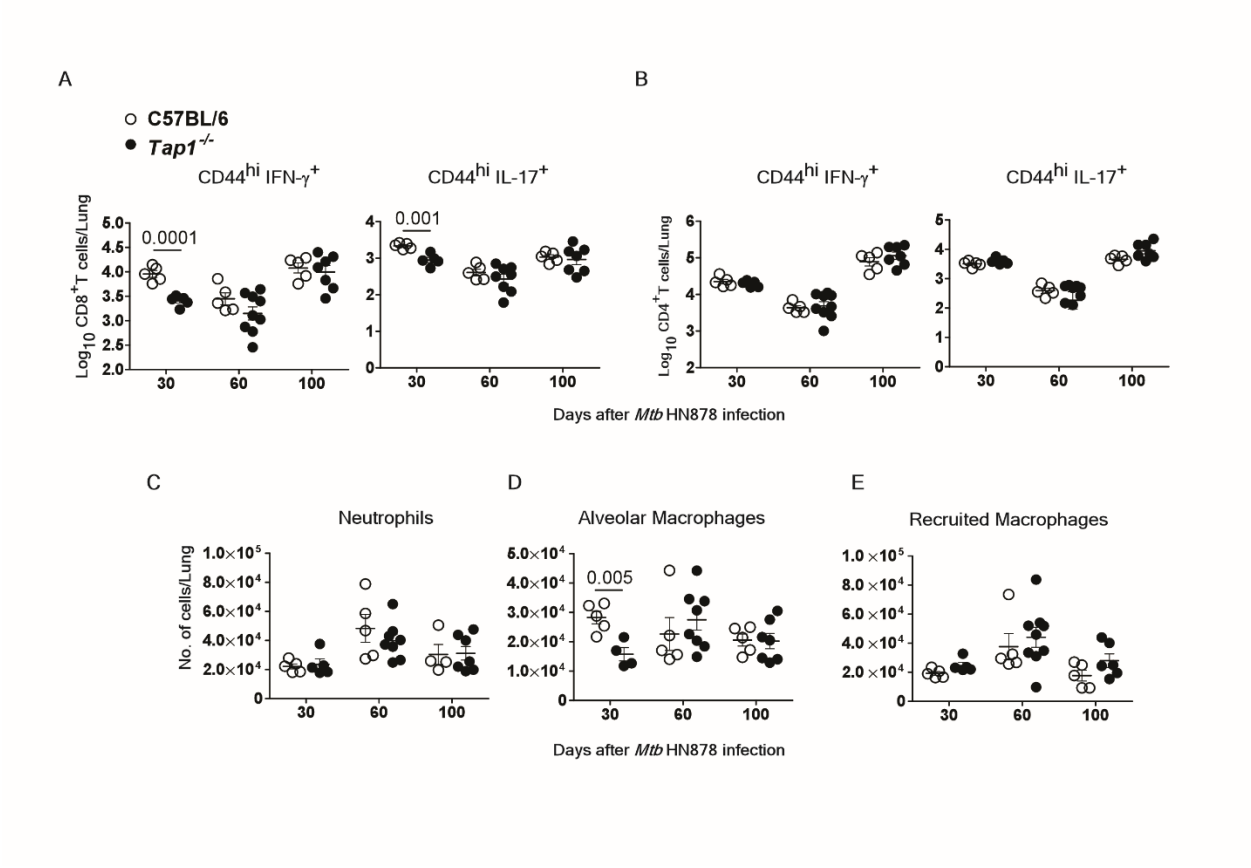

Fig.S3. T cell cytokine profile and myeloid cell recruitment in *Mtb*-infected *Tap1*$^{-/-}$ mice. C57BL/6 or *Tap1*$^{-/-}$ mice were challenged with *Mtb* HN878 (100 CFU) by aerosol route. On 30, 60 and 100 days post-infection (dpi), lungs were harvested for preparation of single cell suspension. Flow cytometry was used to assess, (**A and B**) activated $CD8^+$ and $CD4^+$ T cells and their IFNγ and IL-17 cytokine profiles and (**C-E**) myeloid cell recruitment in the lung. The data points represent the means (±SEM) of one out of 2 separate experiments. *P*-values were determined using unpaired two-tailed Student's t-test between C57BL/6 and *Tap1*$^{-/-}$ mice, at different time points.

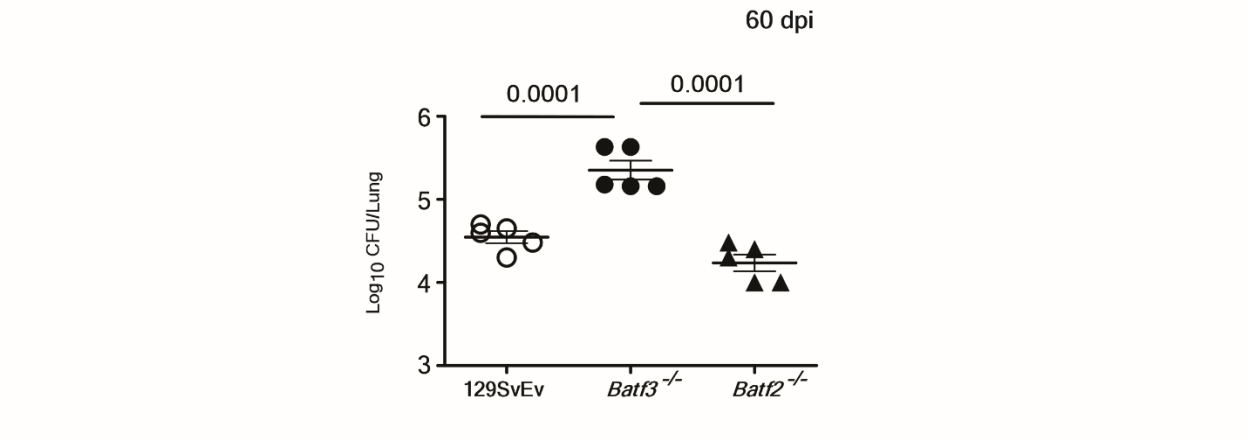

Fig.S4. Protection from *Mtb* HN878 infection is mediated by *Batf2*. 129SvEv, *Batf3*$^{-/-}$ or *Batf2*$^{-/-}$ mice were challenged with *Mtb* HN878 (100 CFU) by aerosol route. Bacterial burden in the lungs of the different strains was determined by plating at 60 dpi. The data points represent the means (±SEM) of one out of two separate experiments. *P*-values between 129SvEv and gene-deficient mice were determined by one-way ANOVA. *P* = 0.04 for unpaired two-tailed Student's t-test between 129SvEv and *Batf2*$^{-/-}$.

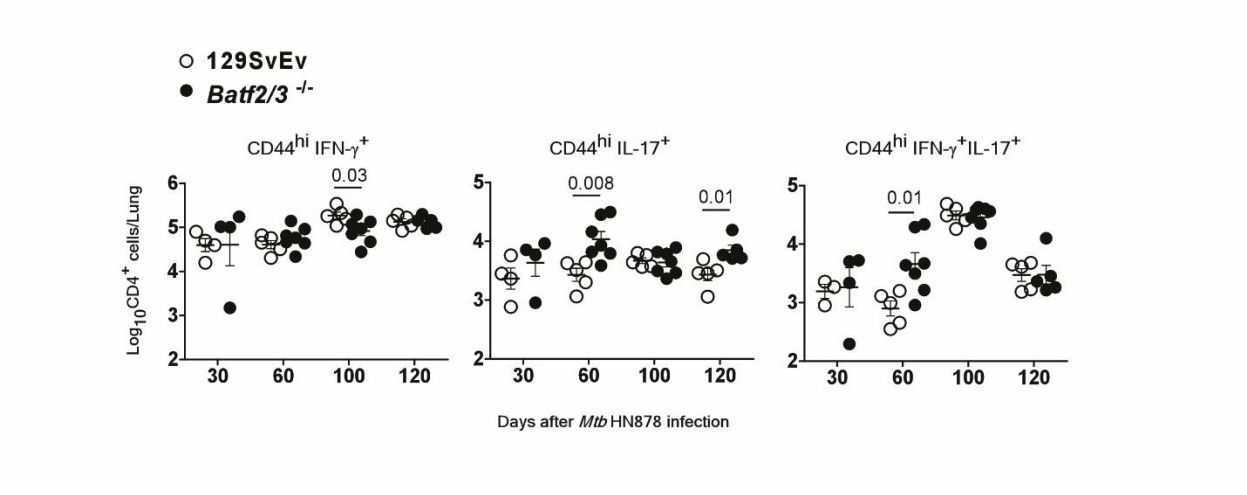

Fig.S5. IL-17-producing CD4$^+$ Th17 cells are increased in *Mtb*-infected *Batf2/3*$^{-/-}$ mice. 129SvEv or *Batf2/3*$^{-/-}$ mice were challenged with *Mtb* HN878 (100 CFU) by aerosol route. Activated CD4$^+$ T cells were assessed for IL-17 and IFNγ profile by flow cytometry. The data points represent the means (±SEM) of one out of two separate experiments. *P*-values between 129SvEv and gene deficient mice were determined by unpaired two-tailed Student's t-test, at different time points.

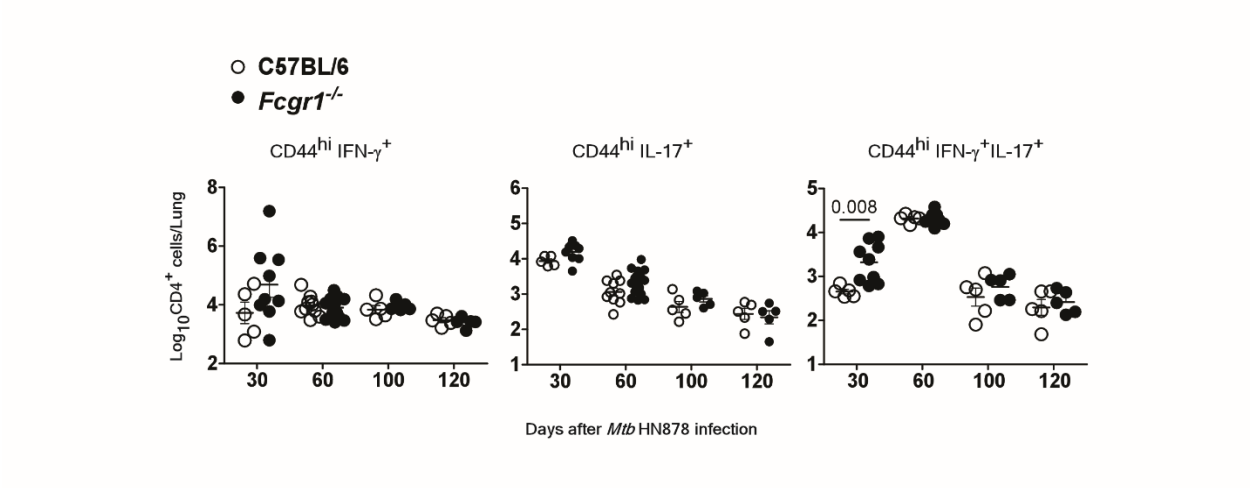

Fig.S6. T cell cytokine profile in *Mtb*-infected *Fcgr1*$^{-/-}$ mice. C57BL/6 or *Fcgr1*$^{-/-}$ mice were challenged with *Mtb* HN878 (100 CFU) by aerosol route. Activated CD4^{+} T cells were assessed for IL17 and IFNγ profile by flow cytometry. The data points represent the means (±SEM) of one out of two separate experiments. *P*-values between C57BL/6 and gene deficient mice were determined by unpaired two-tailed Student's t-test, at different time points.

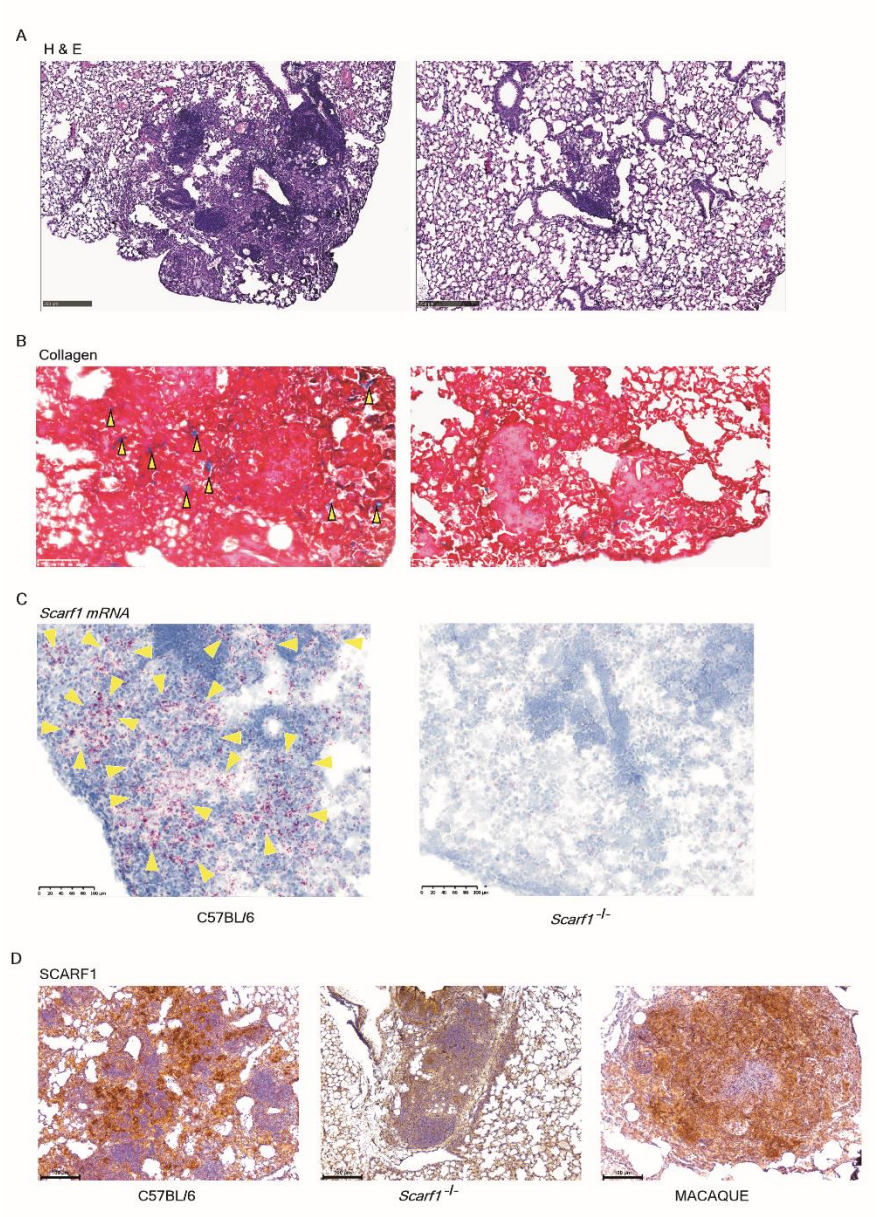

Fig. S7. SCARF1 expression drives inflammation within TB granulomas. *Mtb* HN878-infected lungs from C57BL/6 and *Scarf1*$^{-/-}$ mice at 120 dpi, were processed for (**A**) evaluation of inflammation (by H & E staining), (**B**) collagen production in granulomatous lesions (by Masson's trichrome staining), (**C**) *Scarf1* mRNA localization was determined within FFPE lung sections using RNAScope. Arrows point to *Scarf1* mRNA localization (red) and (**D**) SCARF1 protein expression (by immunohistochemistry) in lung sections from mice and in lung sections from progressor macaques (n=3), one image shown.

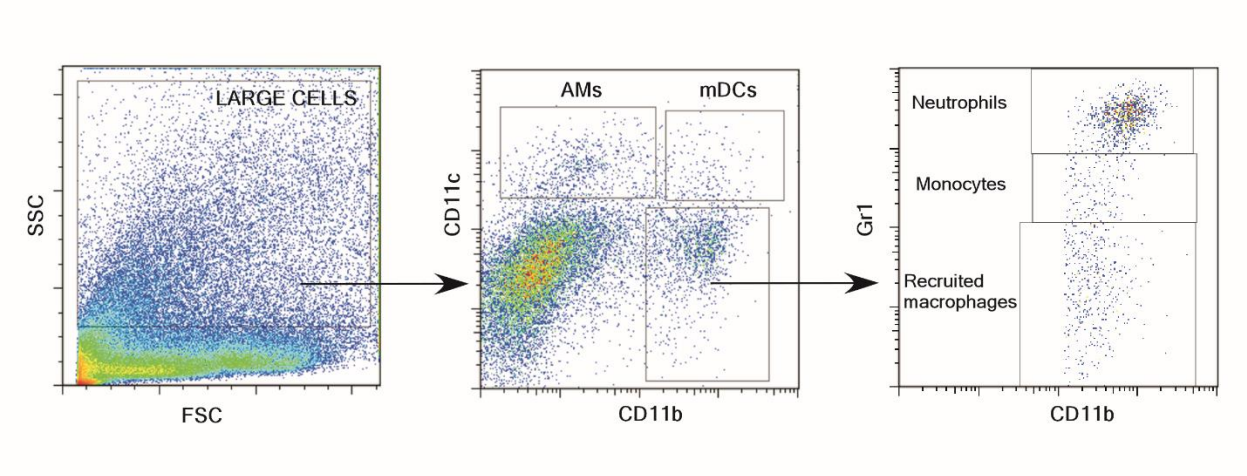

Fig. S8. Hierarchical gating strategy used to identify myeloid populations in mice lungs: C57BL/6 or transgenic mice were aerosol infected with approximately 100 CFU *Mtb* HN878 and lungs were collected at different dpi and flow cytometry analysis was carried out on single-cell suspensions. Alveolar macrophages (AMs) were defined as $CD11c^{+}CD11b^{-}$ cells, myeloid dendritic cells (mDCs) were defined as $CD11c^{+}CD11b^{+}$ cells, neutrophils were defined as $CD11b^{+}CD11c^{-}Gr\text{-}1^{hi}$ cells, monocytes were defined as $CD11b^{+}CD11c^{-}Gr\text{-}1^{med}$ cells, and recruited macrophages were defined as $CD11b^{+}CD11c^{-}Gr\text{-}1^{low}$ cells.

Supplementary Table Titles

Table S1. RNA-Seq sample metadata and accessions.

Table S2. FPKM gene expression values and differential expression statistics for the top 1000 mouse genes, including information about ortholog matches in human and macaque.

Table S3. Significance testing for overlaps of differentially expressed genes between species.

Table S4. Correlation analysis between ACS signature genes and tuberculosis metadata (lung inflammation and bacterial bacteria) among mouse controller and progressor samples.

Table S5. Flow cytometric quantification of lung cellular subsets in control and gene deficient models infected with *Mtb*.

Table S6. Significantly enriched REACTOME pathways among gene sets of interest.